NJC

PAPER

View Article Online
View Journal | View Issue



Cite this: *New J. Chem.*, 2018, **42**, 3633

# Comparative study of $WC_x$-based catalysts for aqueous phase hydrogenolysis of glycerol into bioadditives†

Lingfei Wei,[a] Rehana Bibi,[a] Wei Tian,[a] Lingyu Chen,[a] Yu Zheng,[a] Naixu Li *[a] and Jiancheng Zhou *[abc]

Received 7th December 2017,
Accepted 24th January 2018

DOI: 10.1039/c7nj04844k

rsc.li/njc

Hydrogenolysis of glycerol has been a subject of intensive research in recent decades. Great efforts have been made investigating the mechanism of bond cleavage using metal or metallic oxide catalysts. In this work, effects of a series of $WC_x$-based catalysts, including $WC_x$, $Cu/WC_x$, $Pt/WC_x$, $Ru/WC_x$, $CuRu/WC_x$ and $CuPt/WC_x$, were studied on hydrogenolysis of glycerol to investigate the role of each active phase. $WO_3$-Based catalysts were employed as a comparison with the $WC_x$-based catalysts. Hydrogenolysis of model compounds (1,2-PDO and EG) of glycerol was also studied using these catalysts, in attempts to determine the mechanism of the whole reaction. The presence of metal elements on $WC_x$ or $WO_3$ can significantly improve the conversion of reactant. In addition, the ability of $WC_x$ to promote cleavage of C–C was verified. Ru is more beneficial for formation of EG than Pt, whereas Pt is favorable for formation of 1,2-PDO. It had been supposed that hydrogenolysis of glycerol by $WC_x$-based catalysts occurred *via* two different but overlapping routes: $WC_x$-related reactions caused by C–C cleavage and metal-related reactions caused by C–O cleavage, which happen simultaneously in the reaction. The current study not only demonstrates that the catalytic performance of $WC_x$ can be manipulated by varying metal loading, but also offers a possible mechanism for C–C and C–O cleavage in hydrogenolysis of glycerol, which could be beneficial when focusing on the target product.



## Introduction

As a byproduct of the biodiesel industry, a huge amount of glycerol is produced. The properties of this biomass-derivated substance, such as nontoxicity and sustainability, have driven research into treatments such as hydrogenolysis,[1–3] dehydration,[4–6] reforming,[7–9] acetalization,[10,11] and esterification,[12–14] in attempts to transfer glycerol into important bioadditives thus giving them higher value. Among these, catalytic hydrogenolysis is a promising method for conversion of glycerol into propanediols (PDOs), namely 1,2-propanediol (1,2-PDO) and 1,3-propanediol (1,3-PDO), ethylene glycol(EG), and monohydric alcohol (propanols, methanol, *etc.*). PDOs and EG are industrially important chemicals used as raw materials in production of polymers, surfactants, functional fluids (antifreeze, deicing, dehydrant), resins, cosmetics, and foods.[15,16] Furthermore, propanols (POs, including 1-PO and 2-PO) and methanol are indispensible in daily life as coatings, solvents, cosmetics, pharmaceuticals, and pesticides.

Hydrogenolysis of glycerol involves either a C–C or a C–O cleavage. It is mostly acknowledged that C–C cleavage occurs through a retro-aldol mechanism whereas C–O cleavage occurs by dehydration, which is always affected by base catalysis.[17] Control of the PDOs/EG/monohydric alcohol ratio requires high selectivity of C–O or C–C cleavage of glycerol, which is strongly dependent on the catalyst used.[18] During the reaction, products such as PDOs and EG can be further degraded into substances with smaller molecular weights (such as POs, methanol *etc.*), thus reducing the productivity of the polyalcohol. This reaction process is shown in Scheme 1.[19–21] In this process, glyceraldehyde is an important intermediate that is unstable and elusive, and can subsequently transfer into different products through various pathways (dehydration, hydration *etc.*). The transition of glycerol into glyceraldehyde has been considered to be a metal-promoted reaction, with noble metals such as Pt and Ru showing outstanding performance with the addition of alkali such as NaOH and CaO.[19] EG can be formed from glyceraldehyde through a retro-aldol process or by C–C cleavage of 1,2-PDO. Ru was found to be a good choice by Maris *et al.*[19] and Jian Feng *et al.*,[22] as it shows high selectivity of EG in hydrogenolysis of glycerol.

[a] *School of Chemistry and Chemical Engineering, Southeast University, Nanjing, 211189, P. R. China. E-mail: jczhou@seu.edu.cn*
[b] *Department of Chemical and Pharmaceutical Engineering, Southeast University, Chengxian College, Nanjing, 210088, P. R. China*
[c] *Jiangsu Province Hi-Tech Key Laboratory for Bio-medical Research, Southeast University, Nanjing 211189, P. R. China*

† Electronic supplementary information (ESI) available. See DOI: 10.1039/c7nj04844k

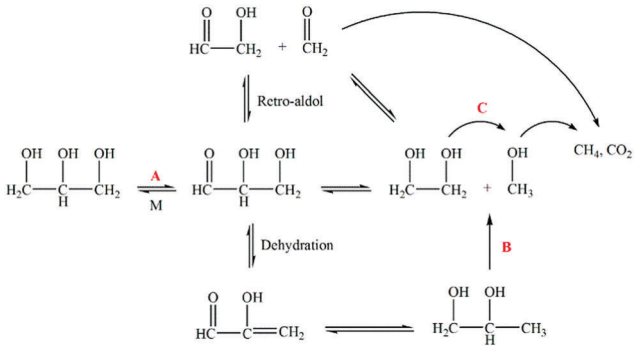


Scheme 1 Mechanism and process of C–C and C–O cleavage in glycerol hydrogenolysis. [a] A, B, C in the scheme shows three main parts in this reaction, which is corresponding to Scheme 2 and will be illustrated in detail hereinafter.

In recent years, transition metal carbides such as tungsten carbides ($WC_x$, $x$ = 0.5, 1) have been identified to have excellent performance in selective C–C and C–O breakage. Zhang Tao's group have done much research on hydrogenation of cellulose with tungsten carbides.[23–25] Ren's team investigated tungsten carbides as selective deoxygenation catalysts, using DFT calculations, surface science experiments, and reactor evaluations. They proved the high activity of the WC(0001) surface towards selective C–O/C=O bond breakage.[26] Bifunctional nickel-containing tungsten carbides have also been found to be very effective for conversion of glucose. High selectivity is derived from the fed-batch system to maintain a certain concentration of sugar solutions, and excellent behavior of metallic nickel component and tungsten component in retro-aldol and hydrogenation processes, respectively.[27]

Accordingly, to better understand how catalysts influence product distribution, investigation is required on the role of each active phase in different reaction parts (part A, B, C). Because of the excellent performance of noble metals Pt and Ru, and non-noble metal Cu in glycerol hydrogenolysis, and the effective bond-breaking ability of $WC_x$ and $WO_3$, this study looks at different loadings (Pt, Ru, Cu or their bimetal) on $WC_x$ or $WO_3$, synthesized by a sol–gel or hydrothermal method, and use of these products in hydrogenolysis of glycerol to explore the role of each active phase. Hydrogenolysis of the model compounds of glycerol (EG and 1,2-PDO) is also discussed to better understand each reaction part. Moreover, on the basis of a previously defined mechanism provided, the effect of each catalyst in the reaction is discussed and a new mechanism based on $WC_x$ is proposed. It should be noted that some side reactions occurred under high temperature, such as aqueous phase reforming and hydrothermal reaction, and these are not considered in the whole study.

# Results and discussion

## Characterization of the catalysts

**Physical properties of the catalysts.** The physical properties of $WC_x$-based and $WO_3$-based catalysts are shown in Table 1.

Table 1 Physical properties of the catalysts

| Catalyst | $S_{BET}$ ($m^2\ g^{-1}$) | $D_{pore}$ (nm) | $V_{pore}$ ($cm^3\ g^{-1}$) |
|---|---|---|---|
| $WC_x$ | 34.7 | 2.804 | 0.024 |
| $Cu/WC_x$ | 28.0 | 5.185 | 0.036 |
| $Pt/WO_3$ | 21.6 | 9.771 | 0.053 |
| $Pt/WC_x$ | 25.7 | 4.455 | 0.029 |
| $Ru/WO_3$ | 26.7 | 8.024 | 0.053 |
| $Ru/WC_x$ | 19.6 | 6.025 | 0.030 |
| $CuPt/WC_x$ | 153.7 | 3.250 | 0.124 |
| $CuRu/WC_x$ | 40.2 | 5.865 | 0.059 |

The BET surface area, pore diameter, and pore volume of $WC_x$ are 34.7 $m^2\ g^{-1}$, 2.804 nm, and 0.024 $cm^3\ g^{-1}$, respectively. For $Cu/WC_x$, $Pt/WC_x$, and $Ru/WC_x$, the BET surface areas are much lower than that of $WC_x$, whereas the pore diameters and pore volumes are larger than those of $WC_x$. This may related to the pore size distribution.[28] For $CuPt/WC_x$ and $CuRu/WC_x$, the BET surface area, pore diameter, and pore volume are both larger than those of $WC_x$, and, notably, $CuPt/WC_x$ possesses the largest BET surface area and pore volume, which can be explained by its apparent porous structure and the plicated surface as shown in the SEM images in Fig. S1 (ESI†). Comparing the physical properties of $WC_x$-based and $WO_3$-based catalysts, it is found that $WC_x$-based catalysts have larger BET surface but lower pore diameter and pore volume than $WO_3$-based catalysts. Composition of each element was measured by ICP-OES (Table S1, ESI†). Differences between theoretical value and effective value may result from experimental bias.

**Structure properties of the catalysts.** Fig. 1 shows XRD patterns of the as-synthesized $WC_x$ under different calcination temperatures (800, 1000, 1200, 1400 °C). Apparently, no crystal forms exist under 800 °C. When the calcination temperature was changed to 1000 °C, there were obvious peaks at around 31.6°, 35.6°, 38.1°, 39.6°, 48.3°, 61.6°, and 73.2°, consistent with the JCPDS cards No. 89-2727 (pure hexagonal WC) and No. 89-2371 (pure orthorhombic $W_2C$). As no peaks for other impurities are found in the pattern, it can be confirmed that the catalyst is a composite of WC and $W_2C$. Diffraction peaks at around 31.6°, 35.6°, 48.3°, and 73.2° are assigned to the (001), (100), (101), and (111) faces of pure hexagonal WC, respectively. Diffraction peaks at around 38.1°, 39.6°, and 61.6° are assigned to the (200), (121), and (040) faces of pure orthorhombic $W_2C$, respectively. Moreover, typical

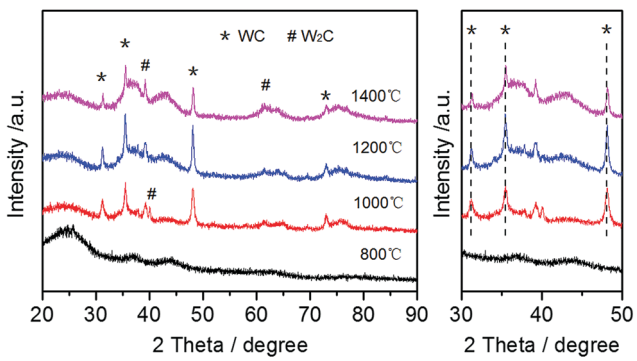


Fig. 1 XRD patterns of $WC_x$ under different temperatures.

 

diffraction peaks of pure orthorhombic $W_2C$ at 34.5°, 52.4°, and 69.8° all missing under each condition, indicate that the high energy surfaces of $W_2C$ phase fall away gradually as the temperature rises, leaving only some low-energy surfaces. The sharpest peaks present at 35.6° and 48.3° of each sample indicate that WC grains synthesized by the sol–gel method under such conditions show (100) and (101) preferred orientations. The intensity of each peak of the WC phase becomes stronger at 1200 °C than at 1000 °C, indicating growing of crystalline grains and a better degree of crystallinity. However, at further increased temperature (1400 °C), peak intensity becomes weak again. This may because of transition of the crystalline phase from WC to $W_2C$ at such high temperatures, speculated from the sharpening of the peak at 38.1° assigned to the (200) face of pure orthorhombic $W_2C$. A detailed study of the predominant 30°–50° reflections showed that rising temperature resulted in a slight shift of WC diffraction peaks toward higher $2\theta$ values. This behavior is indicative of structure defects (lattice contraction) on the surface of WC, caused by the high temperature. This can be corroborated by calculation of the grain size using the Debye–Scherrer equation.[29] The grain size of WC changed from 16.4 Å to 20.7 Å, and 25.7 Å with rising calcination temperature (1000–1400 °C). To obtain a relatively small crystal grain and take energy conservation into consideration, a temperature of 1200 °C was chosen to calcine catalysts in the following steps.

Fig. 2 shows XRD patterns of metal-loaded $WC_x$ catalysts synthesized at 1200 °C. Clearly, when Cu, Ru, CuRu, or CuPt were loaded onto $WC_x$, $WC_x$ remained a composite of WC and $W_2C$, whereas from the Pt-loaded $WC_x$, showing no diffraction peaks of $W_2C$, only the pure WC phase was left. Interestingly, peak intensity of WC and $W_2C$ in the $WC_x$-based catalysts showed the following trend: $Cu/WC_x$ > $CuRu/WC_x$, $CuPt/WC_x$ > $Ru/WC_x$ > $Pt/WC_x$, indicating that the load of noble metals can significantly reduce crystallinity and degree of order of WC or $W_2C$, while the load of Cu is favorable for growing crystalline grains and yielding a better degree of crystallinity. Comparing the patterns of $Cu/WC_x$, $CuRu/WC_x$, and $CuPt/WC_x$, Ru-loaded catalyst shows a relatively weaker peak intensity at 38.1° assigned to the (200) face of pure orthorhombic $W_2C$, indicating that Ru can impair growth of the (200) face of $W_2C$. There are some peaks belonging to carbon shown in the patterns of $Cu/WC_x$, $CuRu/WC_x$, and $CuPt/WC_x$, illustrating that Cu leads to carbon deposition in the calcination process.

The morphologies of the prepared $WC_x$ were characterized by SEM and TEM (Fig. 3). As shown in Fig. 3a, $WC_x$ prepared by the sol–gel method accumulate in clumps and exhibit a scaly-like surface. Fig. 3b shows a more detailed picture, with orderly wrinkles on the surface. Such a blocky structure is stacked up with lattice fringes of 0.284 nm, corresponding to the (001) plane of WC and indicating that $WC_x$ mostly consists of WC in this area. Fig. 3c and d give the TEM image and SAED pattern of another area of the synthetic $WC_x$. Wrinkles can also be seen in Fig. 3c, and electron diffraction (Fig. 3d) confirms the presence of the $W_2C$ phase in this area as the single crystal form. This result that both WC phase and $W_2C$ phase exist in the synthesized catalyst is consistent with results from the XRD experiment. Fig. 4 gives TEM images of $WC_x$-based catalysts. From Fig. 4a and b, Cu particles are distributed on the surface of $WC_x$ and have an average size of 17.22 nm. The lattice fringes exhibited in Fig. 4b are about 0.130 nm, corresponding to the (220) plane of Cu. Similarly, Fig. 4c–f show the particle distribution of Pt and Ru on $WC_x$. EDS spectra also give a rough element content, which is approximate to the theoretical value, implying that the metal has been successfully loaded onto the $WC_x$. TEM images of $CuPt/WC_x$ and $CuRu/WC_x$ are given in Fig. 4g and h. It is interesting that no wrinkles on the surface of $WC_x$ are seen, which may related to the loaded metal. The element content also proved to be approximate to the theoretical value, detected by the EDS spectra. Further confirmation of the existence of each element in $CuPt/WC_x$ and $CuRu/WC_x$ was characterized

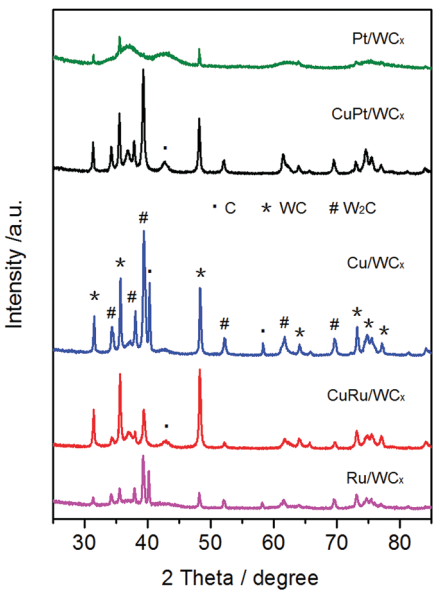


Fig. 2 XRD patterns of $WC_x$-based catalysts (calcined at 1200 °C).

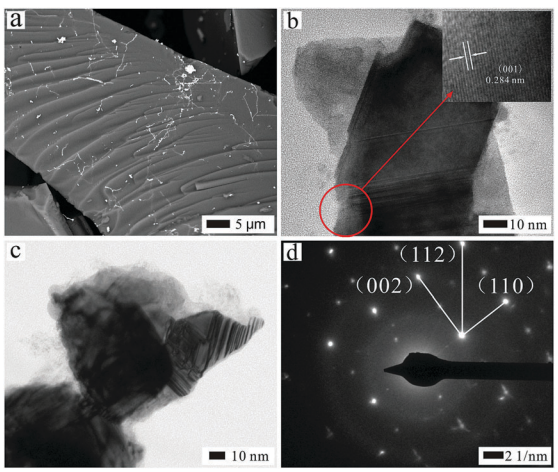


Fig. 3 (a) SEM image of $WC_x$, (b and c) TEM images of $WC_x$. The inset in (b) shows the corresponding HRTEM image to (d) the SAED patterns from the region of $WC_x$ (c).

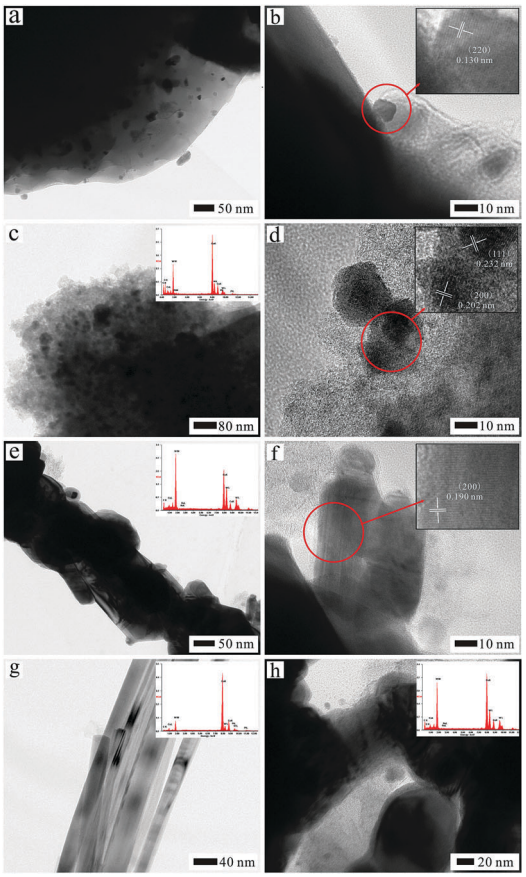


Fig. 4 TEM images of (a and b)[a] Cu/$WC_x$, (c and d) Pt/$WC_x$, (e and f) Ru/$WC_x$, (g)[a] CuPt/$WC_x$, and (h)[a] CuRu/$WC_x$. Insets are the corresponding EDS spectra and HRTEM image. [a] The EDS spectra of Cu/$WC_x$ was ignored because of the use of coated copper grids.

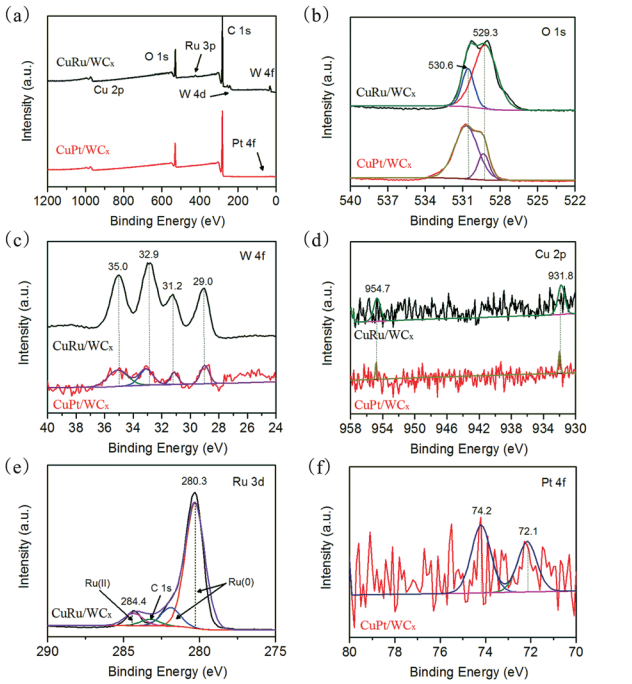


Fig. 5 (a) XPS survey spectra of sample CuRu/$WC_x$ and CuPt/$WC_x$; (b–f) high resolution XPS spectra of O, W, Cu, Ru, and Pt.

by STEM-EDX mapping (Fig. S2 and S3, ESI†). Highly dispersed Cu, Ru, and Pt were observed, and the existence of O could be attributed to adventitious oxygen from the air.

The surface chemical compositions and electronic structure of $WC_x$-based catalysts were investigated by X-ray photoelectron spectroscopy (XPS) (Fig. 5). Fig. 5a provides a comparison of survey spectra of CuRu/$WC_x$ and CuPt/$WC_x$. Both samples show binding energies originating from O 1s, C 1s, W 4f, and Cu 2p. The W 4f spectra for the catalysts (Fig. 5c) are characteristic of WC and $W_2C$ phases. Peaks at binding energies of 31.2 and 29.0 eV belong to the WC phase, corresponding to W $4f_{5/2}$ and W $4f_{7/2}$, respectively. Peaks at binding energies of 32.9 and 35.0 eV belong to the $W_2C$ phase, corresponding to W $4f_{5/2}$ and W $4f_{7/2}$, respectively.[30, 31] This result confirms the fact that both WC and $W_2C$ phases exist in the catalyst, consistent with the XRD and TEM results. Two peaks in Fig. 5d at binding energies around 931.8 and 954.7 eV could be assigned to Cu $2p_{3/2}$ and Cu $2p_{1/2}$, respectively, corresponding to the metallic Cu (Cu(0)) species.[32, 33] The Ru 3d and Pt 4f spectra for the CuRu/$WC_x$ and CuPt/$WC_x$ catalysts are shown in Fig. 5e and f, respectively. In the XPS of Ru systems, the referencing of the binding energy scale is complicated by the superposition of the C 1s and the Ru 3d signals. Fig. 5e shows a Ru $3d_{5/2}$ signal at 280.3 eV, attributed to Ru(0). The Ru $3d_{3/2}$ and $3d_{5/2}$ peaks appear separated by approximately 4.2 eV, consistent with the literature records.[34] Fig. 5f shows the Pt 4f peaks of CuPt/$WC_x$. Two peaks at around 72.1 and 74.2 eV correspond to Pt(0) and Pt(IV), respectively,[35,36] which illustrates that the metallic Pt is not the only species to exist in the catalyst.

## Catalytic performance of the catalysts

The carbon mass balance was calculated (Table S2, ESI†), and the conversion calculated by glycerol weight (con. by weight%). The difference between the two conversions is tentatively regarded as the amount of carbon-containing gases produced from glycerol hydrogenolysis. Results show that about 60–80% of the total carbon put into the reactor remains in the liquid product, demonstrating that the cellulose was predominantly converted into liquid products. Table 2 summarizes the results of hydrogenolysis of glycerol/EG/1,2-PDO under $WC_x$-based and $WO_3$-based catalysts ($WC_x$, Cu/$WC_x$, Pt/$WO_3$, Pt/$WC_x$, Ru/$WO_3$, Ru/$WC_x$, CuPt/$WC_x$, and CuRu/$WC_x$), including the conversion of reactant and selectivity of each product. As shown by runs #1, 4, 7, 10, 13, 16, 19, and 22 in Table 2, in the reaction of hydrogenolysis of glycerol, tungsten-based catalysts showed good performance in converting glycerol into dihydric alcohol or monohydric alcohol. In each reaction, conversion of glycerol was no less than 64.9% and reached up to 84.5% under the catalysis of CuRu/$WC_x$, suggesting that CuRu/$WC_x$ may be the preferred choice to convert glycerol. However, it is more complicated when the selectivity of each product is considered. It can be seen in run #1 that when $WC_x$ is taken as the single active phase, the main products of hydrogenolysis of glycerol are methanol and EG, occupying selectivity of 19.6% and 25.2%, respectively,

 

Table 2 Summary of reactant conversion and product selectivity during hydrogenolysis of glycerol/EG/1,2-PDO[a,b,c,d]

| Run# | Catalyst | Reactant | Conversion (%) | Selectivity (%) | | | | | |
|---|---|---|---|---|---|---|---|---|---|
| | | | | Methanol | 1-PO | 2-PO | 1,2-PDO | EG | 1,3-PDO |
| 1 | $WC_x$ | Glycerol | 64.9 | 19.6 | 2.9 | 3.0 | 10.3 | 25.2 | 11.4 |
| 2 | $WC_x$ | EG | 43.7 | 16.7 | — | — | — | — | — |
| 3 | $WC_x$ | 1,2-PDO | 41.3 | 7.0 | 1.2 | 2.8 | — | 24.0 | — |
| 4 | $Cu/WC_x$ | Glycerol | 72.0 | 13.3 | 1.1 | 3.8 | 10.1 | 19.6 | 37.2 |
| 5 | $Cu/WC_x$ | EG | 60.2 | 19.3 | — | — | — | — | — |
| 6 | $Cu/WC_x$ | 1,2-PDO | 54.3 | 12.2 | 29.5 | 11.1 | — | 15.4 | — |
| 7 | $Pt/WO_3$ | Glycerol | 74.4 | 3.1 | 3.0 | 4.6 | 30.8 | 8.6 | 8.1 |
| 8 | $Pt/WO_3$ | EG | 83.0 | 9.8 | — | — | — | — | — |
| 9 | $Pt/WO_3$ | 1,2-PDO | 57.8 | 18.9 | 22.3 | 19.8 | — | 12.5 | — |
| 10 | $Pt/WC_x$ | Glycerol | 79.2 | 12.3 | 4.7 | 0.9 | 39.3 | 19.7 | 19.9 |
| 11 | $Pt/WC_x$ | EG | 80.7 | 19.3 | — | — | — | — | — |
| 12 | $Pt/WC_x$ | 1,2-PDO | 57.8 | 18.3 | 30.2 | 8.0 | — | 13.9 | — |
| 13 | $Ru/WO_3$ | Glycerol | 73.5 | 0.3 | 0.2 | 4.9 | 22.9 | 20.0 | 5.4 |
| 14 | $Ru/WO_3$ | EG | 67.4 | 4.9 | — | — | — | — | — |
| 15 | $Ru/WO_3$ | 1,2-PDO | 48.9 | 22.3 | 14.7 | 18.7 | — | 21.9 | — |
| 16 | $Ru/WC_x$ | Glycerol | 84.3 | 10.7 | 2.5 | 2.2 | 10.5 | 61.6 | 3.3 |
| 17 | $Ru/WC_x$ | EG | 30.3 | 24.5 | — | — | — | — | — |
| 18 | $Ru/WC_x$ | 1,2-PDO | 66.2 | 10.7 | 28.1 | 4.2 | — | 33.2 | — |
| 19 | $CuPt/WC_x$ | Glycerol | 80.2 | 3.7 | 3.8 | 5.3 | 49.7 | 21.7 | 13.2 |
| 20 | $CuPt/WC_x$ | EG | 84.2 | 10.6 | — | — | — | — | — |
| 21 | $CuPt/WC_x$ | 1,2-PDO | 48.9 | 17.7 | 32.8 | 10.9 | — | 17.2 | — |
| 22 | $CuRu/WC_x$ | Glycerol | 84.5 | 0.5 | 13.3 | 9.2 | 45.6 | 19.8 | 8.4 |
| 23 | $CuRu/WC_x$ | EG | 86.5 | 14.4 | — | — | — | — | — |
| 24 | $CuRu/WC_x$ | 1,2-PDO | 68.4 | 1.5 | 44.4 | 11.9 | — | 24.9 | — |

[a] Each value was obtained after 8 h reaction with the same $H_2$ pressure (4 MPa) and catalyst amount (0.15 g). [b] Each reaction was performed three times and values were obtained as the mean value. [c] Gas products were released after the reaction, but ignored in calculation. [d] Data in the table include only the six main products, therefore numbers not totalling 100% can be explained by several unnameable products in trace amounts, which were ignored intentionally.

indicating $WC_x$ itself has good C–C cleavage ability. Compare run #1 with runs #4, 10, and 16, and a remarkable enhancement in glycerol conversion is found, illustrating that metal loading has a positive promotion effect on glycerol conversion and that $Ru/WC_x$ appears to be more active than $Pt/WC_x$ and $Cu/WC_x$ for hydrogenolysis of glycerol. This result is consistent with other studies comparing the activity of Ru- and Pt-based catalysts for hydrogenolysis of glycerol.[19,37–39] By analyzing data on selectivity, $Ru/WC_x$ exhibited a better tendency to transfer glycerol into EG than $Pt/WC_x$ and $Cu/WC_x$, while $Pt/WC_x$ and $Cu/WC_x$ revealed significant 1,2-PDO and 1,3-PDO formation. Selectivity of methanol also occupied an appreciable portion when $Cu/WC_x$, $Pt/WC_x$, or $Ru/WC_x$ were used as the catalyst, which may because of the ability of transition metal carbides to cleave C–C bonds. Comparing runs #7 and 13 in Table 2, having almost the same glycerol conversion, $Pt/WO_3$ promoted 30.76% selectivity to 1,2-PDO with only 8.6% selectivity to EG, while $Ru/WO_3$ promoted 22.9% selectivity to 1,2-PDO with 20.0% selectivity to EG. Runs #10 and 16 showed that selectivity of 1,2-PDO and EG was 39.3% and 19.7%, respectively, with catalysis of $Pt/WC_x$, 10.5% and 61.6%, respectively, with catalysis of $Ru/WC_x$. The obvious differences also imply that Ru is more beneficial for formation of EG than Pt, whereas Pt is favorable for formation of 1,2-PDO. When comparing runs #19 and 22, selectivity of 1,2-PDO remained high both with $CuPt/WC_x$ (49.7%) or $CuRu/WC_x$ (45.6%), but much of the EG and 1,2-PDO were transferred into POs with catalysis of $CuRu/WC_x$, compared with $CuPt/WC_x$.

The catalytic activity of Cu in hydrogenolysis of glycerol was studied in runs #1 and 4, runs #10 and 19, runs #16 and 22 (Table 2). Compared with run #1, a relatively high selectivity of 1,3-PDO (37.2%) was obtained in run #4, indicating that when Cu participates in the form of a single loaded metal ($Cu/WC_x$), it can significantly improve the ability of glycerol transfer into 1,3-PDO. In runs #10 and 19, runs #16 and 22, in which Cu and a noble metal (Pt and Ru) were added as a bi-metal loaded onto $WC_x$, selectivity of 1,2-PDO all increased more than 10%. Furthermore, selectivity of EG showed a sharp decline when $CuRu/WC_x$ was used in the reaction compared with $Ru/WC_x$. Clearly, a favorable C–O cleavage pathway exists on Cu. In addition, comparing run #4 with run #19 and 22, participation of Pt or Ru, respectively, in the catalyst system caused higher selectivity of 1,2-PDO, and decline of selectivity of methanol and 1,3-PDO at the same time. This could be because of subsequent hydrogenolysis of EG and 1,2-PDO under the different catalysts, and will be discussed in the following text. Results from use of $WC_x$-based catalysts and $WO_3$-based catalysts were also considered. From runs #7 and 10, conversion of glycerol is much higher with $Pt/WC_x$, and selectivity of methanol and EG were also higher, compared with the $Pt/WO_3$ catalyzed reaction. Similar results were also obtained from runs #13 and 16, confirming that $WC_x$ has much better ability to transfer glycerol and promote cleavage of C–C over C–O.

Using the same method, the catalytic influence on hydrogenolysis of EG and 1,2-PDO was studied. Results show that (i) metal-loaded $WC_x$ are preferable to enhance conversion of EG/1,2-PDO. Among these, the highest conversions were obtained by $CuRu/WC_x$, 86.5% for hydrogenolysis of EG and 68.4% for hydrogenolysis of 1,2-PDO; (ii) $Cu/WC_x$, $Pt/WC_x$, and $Ru/WC_x$

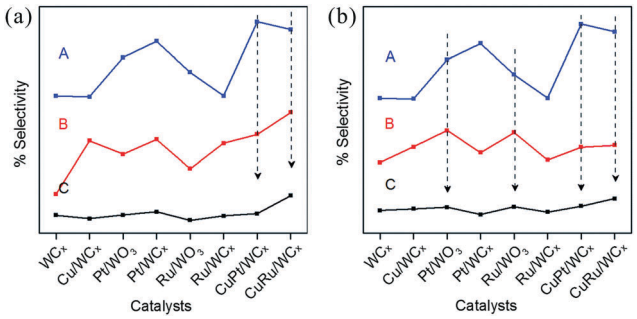


Fig. 6 (a) Selectivity of 1,2-PDO or 1-PO with different catalysts, (b) selectivity of 1,2-PDO or 2-PO with different catalysts. A, B and C refer to selectivity of 1,2-PDO in glycerol hydrogenolysis, selectivity of 1-PO (a) or 2-PO (b) in 1,2-PDO hydrogenolysis and selectivity of 1-PO (a) or 2-PO (b) in glycerol hydrogenolysis, respectively.

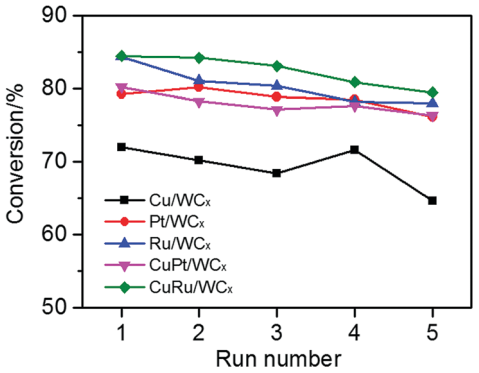


Fig. 7 Recycling of WC$_x$-based catalysts in hydrogenolysis of glycerol.

exhibited higher selectivity of methanol in hydrogenolysis of EG compared with other catalysts, which may because of the good C–C cleavage ability of WC$_x$. CuPt/WC$_x$ and CuRu/WC$_x$ did not show such tendencies, perhaps because of the large area coverage of metals on the surface of WC$_x$, which can decrease the active sites of WC$_x$; (iii) the main product of hydrogenolysis of 1,2-PDO is 1-PO, metal-loaded catalysts can significantly improve the selectivity of 1-PO. Among these, CuRu/WC$_x$ showed the most inclination to transfer 1,2-PDO into 1-PO.

As discussed, WC$_x$ specializes in C–C cleavage, thus showing high selectivity of methanol both in EG and 1,2-PDO hydrogenolysis. In this case, selectivity of methanol in glycerol hydrogenolysis exhibits a relatively high value. The same tendency is found when referring to selectivity of 1-PO or 2-PO. As shown in Fig. 6, high selectivity of 1,2-PDO in glycerol hydrogenolysis and high selectivity of 1-PO (in Fig. 6a) or 2-PO (in Fig. 6b) in 1,2-PDO hydrogenolysis caused high selectivity of 1-PO (in Fig. 6a) or 2-PO (in Fig. 6b) in glycerol hydrogenolysis. On the contrary, when Ru/WC$_x$ was used as the catalyst, 33.2% selectivity of EG was obtained in hydrogenolysis of 1,2-PDO, and with a relatively high conversion of 1,2-PDO (66.2%), a considerable amount of the product 1,2-PDO was subsequently transferred into EG in glycerol hydrogenolysis with Ru/WC$_x$. Meanwhile, only 30.3% of EG was transferred into methanol, thus the selectivity of EG can reach up to 61.6% in hydrogenolysis of glycerol while selectivity of 1,2-PDO reaches only 10.5%. This trend is found with other catalysts (Fig. 6), highlighting the importance of consideration of catalytic effects on side reactions in order to get a certain product.

### Recycling stability

After each reaction, catalysts were recollected and washed with deionized water several times, followed by drying at 80 °C for 12 h. X-ray diffraction was used to characterize the structure of catalysts after the reaction (Fig. S5, ESI†). It is clear that all catalysts after reaction retain a fine lattice structure, including diffraction peaks both of WC and $W_2C$, along with several small peaks of graphite carbon. Peak intensity of Pt/WC$_x$ and Ru/WC$_x$ both increased compared with intensity before the reaction, indicating growth of crystalline grains and a better degree of crystallinity. Recycling stability was also examined (Fig. 7). Although the general tendency of glycerol conversion with each catalyst is decline within five runs, the drop rate is quite slight compared with the highest value. Among the five catalysts, Cu/WC$_x$ seems to have the poorest reusability (declined about 7.3%), whereas Pt/WC$_x$ and CuPt/WC$_x$ possess the best reusability (declined about 3.1% and 3.9%, respectively). It was considered that deactivation of catalysts results from loss of the W element in the reused catalysts,[27] as a decline of W content was detected by ICP-OES (Fig. S6, ESI†). Results also show that the amount of loaded metal decreased after each run. It was assumed that loaded metal elements can drop out easily from the original support and fall into solution during reaction, which may be another reason for deactivation of catalysts.

## Discussion

From the results, it can be concluded that metal and WC$_x$ both play efficient roles in the reactions. The metal and WC$_x$ may have distinct routes to interact with the reactant, and a suggested mechanism is shown in Scheme 2. Hydrogenolysis of glycerol can be divided into three parts: A, B, and C, which represent reactions in glycerol, 1,2-PDO, and EG, respectively. Each part includes WC$_x$-related reactions, *i.e.* C–C cleavage (route A), and metal-related reactions, *i.e.* C–O cleavage (route B).

Active hydrogen species can be produced under high temperature with a metal catalyst, plenty of free $H^+$ filled in the reaction system and bonded with –OH that link to the terminal carbon or the center carbon in glycerol (called $C_1$ in this article). In route A processes, the increase of electron cloud density of $C_1$ caused another shift of electron cloud between two adjacent carbon atoms (called $C_2$ or $C_3$ in this study, shift of electron cloud in the way of $C_1$–$C_2$–$C_3$ or $C_1$–$C_2$). In this process, a carbon with positive electricity must be produced and this would be attracted to the carbon with negative electricity in the WC$_x$-based catalyst exposed on the catalyst surface. Because of the strong attraction between the carbon atom and tungsten atoms in the catalyst system, cleavage of C–C can only occur in glycerol thus forming a dihydric alcohol (EG) and a monohydric alcohol (methanol). Similarly, a route B process occurs simultaneously, indicating a C–O cleavage process through dehydration, and forming 1,2-PDO

 

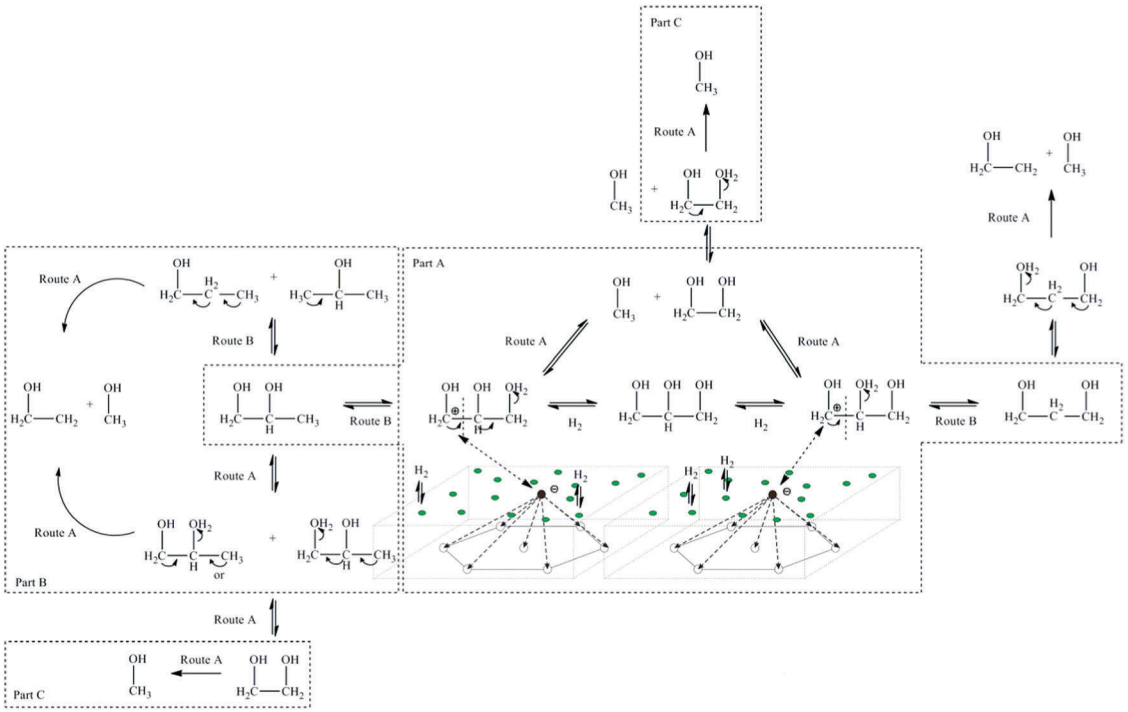


Scheme 2 Possible mechanism for hydrogenolysis of glycerol with $WC_x$-based catalysts. [a] Parts A, B, C represent three different reactions with reactants of glycerol, 1,2-PDO, and EG, respectively. [b] Route A represents $WC_x$-related reactions caused by C–C cleavage and route B represents metal-related reactions caused by C–O cleavage. [c] Green dots in the scheme represent the loaded metals on the surface of $WC_x$.

and 1,3-PDO.[37, 39, 40] Part B shows a reaction of 1,2-PDO, including route A and route B, and forms products with small molecules such as 1-PO, 2-PO, EG, ethanol, and methanol. Similarly, part C shows a subsequent reaction of EG, which produced methanol as its main product.

As discussed, $Pt/WC_x$ and $Ru/WC_x$ showed good performance in hydrogenolysis of glycerol into EG (line A in Fig. 8). $Cu/WC_x$, $Pt/WC_x$, and $Ru/WC_x$ all exhibited good performance in hydrogenolysis of EG into methanol (line B in Fig. 8). Correspondingly, selectivity of methanol also showed a relatively high value in hydrogenolysis of glycerol under $Cu/WC_x$, $Pt/WC_x$, and $Ru/WC_x$ (line C in Fig. 8). This process (from glycerol to EG and then to methanol) was catalyzed mainly by $WC_x$ through route A, thus $WO_3$-based catalysts did not show such tendencies. However, the reasons $CuPt/WC_x$ and $CuRu/WC_x$ did not show such tendencies remain unclear. This may be because of competition between $WC_x$-related reactions and metal-related reactions. Further factors in the two routes are under study.

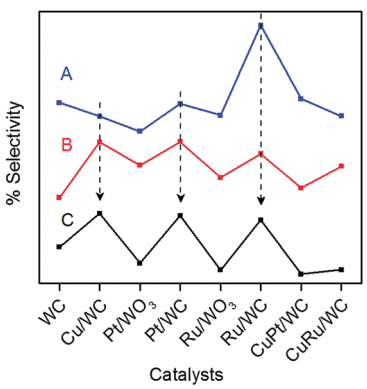


Fig. 8 Selectivity of EG in hydrogenolysis of glycerol (A), selectivity of methanol in hydrogenolysis of EG (B), and selectivity of methanol in hydrogenolysis of glycerol (C).

# Experimental

## Chemicals and materials

Ammonium tungstate hydrate ($H_{40}N_{10}O_{41}W_{12}{\cdot}H_2O$, 99.0%), citric acid monohydrate ($C_6H_8O_7{\cdot}H_2O$, 99.8%), sucrose ($C_{12}H_{22}O_{11}$,), ammonium platinic chloride ($(NH_4)_2PtCl_6$, 99.8%), ruodium chloride hydrate ($RuCl_3{\cdot}xH_2O$, 99.6%), copper nitrate trihydrate ($Cu(NO)_3{\cdot}3H_2O$, 99.8%), and sodium borohydride ($NaBH_4$, 99.8%) were all purchased from the Sinopharm Chemical Reagent Company in analytical grade, and used as received without further purification. Deionized water, with a resistivity of 18.2 MΩ cm, was used throughout the whole experiment.

## Catalyst preparation

**Synthesis of $WC_x$.** $WC_x$ was prepared by a simple sol–gel method, in two parts: preparation of gel precursor and reduction carbonization under high temperature. Ammonium tungstate hydrate (3.0 g, 1 mmol) was dissolved in 50 ml deionized water and stirred for 10 min, followed by addition of a certain amount of citric acid monohydrate under continuous stirring until it became transparent and homogeneous. This solution was than blended with a sucrose aqueous solution to provide carbon in

the reduction carbonization process and mixed uniformly using an ultrasonic machine. The obtained solution was then evaporated off the solvent at 80 °C and dried at 140 °C overnight to get an expanded crumbly solid, which was subsequently ground into a fine powder that was called the gel precursor. After that, the gel precursor underwent a reduction carbonization process, that was calcined under a specific temperature (800, 1000, 1200, 1400 °C) in a temperature programmed tube furnace for 3 h under an Ar and $Ar/H_2$ atmosphere. After cooling to room temperature, the solid sample was collected and stored in a desiccator for further characterization and use.

**Synthesis of $WC_x$-based catalysts.** Similar processes to those used for $WC_x$ were used to synthesize monometallic/bimetallic-loaded $WC_x$, except a specific metallic salt solution or mixture was added and reduced by a $NaBH_4$ solution before blending with the sucrose aqueous solution. All $WC_x$-based catalysts were 1% mass content of each metal element. $WO_3$-Based catalysts were prepared by a hydrothermal method according to a previous report,[41,42] which is not described here.

### Catalyst characterization

Surface area ($S_{BET}$) was calculated using the Brunauer, Emmett, and Teller (BET) method. Pore size distribution and average pore diameter were calculated using the desorption branch of the isotherm according to the Barrett–Joyner–Halenda (BJH) method. The chemical composition of the samples was analyzed using an inductively coupled plasma optical emission spectrometer (ICP-OES, Varian ICP-OES 720). The structure and morphology of the samples were characterized by X-ray diffraction (XRD, Bruker D8-Discover with Cu-Kα radiation, $\lambda$ = 1.5478 Å), scanning electron microscopy (SEM, JSM-7800F), and transmission electron microscopy (TEM, Hitachi H-600, FEI Tecnai G2 F30). X-ray photoelectron spectroscopy (XPS) was measured on a 2000 XPS system with a monochromatic Al-Kα source and a multichannel detector to determine the surface chemical states.

### Activity test

Hydrogenolysis of glycerol and its model compounds (EG and 1,2-PDO) were performed in a stainless-steel micro-autoclave (YZ-MR-100ML) reactor. Typically, 40 ml of 20 wt% glycerol/EG/1,2-PDO aqueous solution was prepared in a quartz cup and 0.15 g catalyst was added to the solution, which was subsequently mixed homogeneously using a ultrasonic machine for 10 min. After that, the quartz cup was put into a stainless-steel micro-autoclave reactor, the reactor was sealed and flushed three times with $N_2$. Then 4 MPa of $H_2$ was injected into the reaction vessel and heated to 220 °C by increasing the temperature gradually, then maintained for 8 h under magnetic stirring at 800 rpm. After the reaction, the autoclave was cooled to room temperature naturally, followed by the release of gas and collection of the liquid product. The liquid product was centrifuged at 8000 rpm and filtrated using the 0.22 μm PES filter membrane. Solid catalyst was collected for further characterization and recycling tests. The pure liquid product was injected into a gas chromatographer (GC, Shanghai Qiyang Info Technology Co., Ltd, China) equipped with a capillary column (ON-WAX, 30 m × 0.32 mm) and a flame ionization detector. Similarly, products were also identified by GC-MS (Shimadzu, GC-MS QP 2010 Plus). The conversion of glycerol/EG/1,2-PDO and selectivity of each product were calculated based on the following equations:

$$\text{Conversion}\,(\%) = \frac{\text{moles of reactant (in)} - \text{moles of reactant (out)}}{\text{moles of reactant (in)}} \times 100\% \quad (1)$$

$$\text{Selectivity}\,(\%) = \frac{\text{moles of one product}}{\text{moles of all liquid products}} \times 100\% \quad (2)$$

## Conclusions

In this work, a series of $WC_x$-based catalysts were prepared and applied to hydrogenolysis of glycerol, as well as its model compounds 1,2-PDO and EG. The presence of metal elements on $WC_x$ or $WO_3$ was proven to significantly improve the conversion of reactant. Ru is more beneficial for formation of EG, whereas Pt is favorable for formation of 1,2-PDO. $WC_x$ was also verified to possess good ability for C–C cleavage. $WC_x$-Related reactions caused by C–C cleavage and metal-related reactions caused by C–O cleavage occurred simultaneously in this process.

## Conflicts of interest

There are no conflicts to declare.

## Acknowledgements

This work was financially supported by the Fundamental Research Funds for the Central Universities of China (No. 3207045403, 3207045409, 3207046414), National Natural Science Foundation of China (No. 21576050 and 51602052), Jiangsu Provincial Natural Science Foundation of China (BK20150604), and a Project Funded by the Priority Academic Program Development of Jiangsu Higher Education Institutions (PAPD).

## Notes and references

1 Z. Yuan, L. Wang, J. Wang, S. Xia, P. Chen, Z. Hou and X. Zheng, *Appl. Catal., B*, 2011, **101**, 431–440.
2 M. L. Barbelli, G. F. Santori and N. N. Nichio, *Bioresour. Technol.*, 2012, **111**, 500–503.
3 S. Zhu, Y. Zhu, S. Hao, H. Zheng, T. Mo and Y. Li, *Green Chem.*, 2012, **14**, 2607–2616.
4 C. W. Chiu, M. A. Dasari, G. J. Suppes and W. R. Sutterlin, *AIChE J.*, 2006, **52**, 3543–3548.
5 W. Suprun, M. Lutecki, T. Haber and H. Papp, *J. Mol. Catal. A: Chem.*, 2009, **309**, 71–78.

 

6 H. Atia, U. Armbruster and A. Martin, *J. Catal.*, 2008, **258**, 71–82.
7 P. D. Vaidya and A. E. Rodrigues, *Chem. Eng. Technol.*, 2009, **32**, 1463–1469.
8 E. L. Kunkes, R. R. Soares, D. A. Simonetti and J. A. Dumesic, *Appl. Catal., B*, 2009, **90**, 693–698.
9 A. O. Menezes, M. T. Rodrigues, A. Zimmaro, L. E. Borges and M. A. Fraga, *Renewable Energy*, 2011, **36**, 595–599.
10 M. S. Khayoon and B. H. Hameed, *Appl. Catal., A*, 2013, **464**, 191–199.
11 S. B. Umbarkar, T. V. Kotbagi, A. V. Biradar, R. Pasricha, J. Chanale, M. K. Dongare and E. Payen, *J. Mol. Catal. A: Chem.*, 2009, **310**, 150–158.
12 S. Zhu, Y. Zhu and X. Gao, *et al.*, *Bioresour. Technol.*, 2013, **130**, 45–51.
13 S. Zhu, X. Gao, F. Dong, Y. Zhu, H. Zheng and Y. Li, *J. Catal.*, 2013, **306**, 155–163.
14 M. S. Khayoon and B. H. Hameed, *Appl. Catal., A*, 2012, **433**, 152–161.
15 S. Zhu, X. Gao, Y. Zhu, Y. Zhu, H. Zheng and Y. Li, *J. Catal.*, 2013, **303**, 70–79.
16 X. Luo, X. Ge, S. Cui and Y. Li, *Bioresour. Technol.*, 2016, **215**, 144–154.
17 D. G. Lahr and B. H. Shanks, *Ind. Eng. Chem. Res.*, 2003, **42**, 5467–5472.
18 S. García-Fernández, I. Gandarias, J. Requies, M. B. Güemez, S. Bennici, A. Auroux and P. L. Arias, *J. Catal.*, 2015, **323**, 65–75.
19 E. P. Maris and R. J. Davis, *J. Catal.*, 2007, **249**, 328–337.
20 D. K. Sohounloue, C. Montassier and J. Barbier, *React. Kinet. Catal. Lett.*, 1983, **22**, 391–397.
21 C. Montassier, J. C. Menezo, L. C. Hoang, C. Renaud and J. Barbier, *J. Mol. Catal.*, 1991, **70**, 99–110.
22 J. Feng, H. Fu, J. Wang, R. Li, H. Chen and X. Li, *Catal. Commun.*, 2008, **9**, 1458–1464.
23 N. Ji, T. Zhang, M. Zheng, A. Wang, H. Wang, X. Wang and J. G. Chen, *Catal. Today*, 2009, **147**, 77–85.
24 A. Wang and T. Zhang, *Acc. Chem. Res.*, 2013, **46**, 1377–1386.
25 S. Van de Vyver, J. Geboers, P. A. Jacobs and B. F. Sels, *ChemCatChem*, 2011, **3**, 82–94.
26 H. Ren, Y. Chen, Y. Huang, W. Deng, D. G. Vlachos and J. G. Chen, *Green Chem.*, 2014, **16**, 761–769.
27 R. Ooms, M. Dusselier, J. A. Geboers, B. O. de Beeck, R. Verhaeven, E. Gobechiya and B. F. Sels, *Green Chem.*, 2014, **16**, 695–707.
28 C. Leyva, M. S. Rana and J. Ancheyta, *Catal. Today*, 2008, **130**, 345–353.
29 L. K. De Souza, J. R. Zamian, G. N. da Rocha Filho, L. E. Soledade, I. M. dos Santos, A. G. Souza and C. E. da Costa, *Dyes Pigm.*, 2009, **81**, 187–192.
30 M. B. Zellner and J. G. Chen, *Catal. Today*, 2005, **99**, 299–307.
31 M. D. Abad, M. A. Muñoz-Márquez, S. El Mrabet, A. Justo and J. C. Sánchez-López, *Surf. Coat. Technol.*, 2010, **204**, 3490–3500.
32 T. Ghodselahi, M. A. Vesaghi, A. Shafiekhani, A. Baghizadeh and M. Lameii, *Appl. Surf. Sci.*, 2008, **255**, 2730–2734.
33 M. C. Biesinger, L. W. Lau, A. R. Gerson and R. S. C. Smart, *Appl. Surf. Sci.*, 2010, **257**, 887–898.
34 V. Mazzieri, F. Coloma-Pascual, A. Arcoya, P. C. L'Argentière and N. S. Fí, *Appl. Surf. Sci.*, 2003, **210**, 222–230.
35 F. B. Li and X. Z. Li, *Chemosphere*, 2002, **48**, 1103–1111.
36 C. Nethravathi, E. A. Anumol, M. Rajamathi and N. Ravishankar, *Nanoscale*, 2011, **3**, 569–571.
37 M. A. Dasari, P. P. Kiatsimkul, W. R. Sutterlin and G. J. Suppes, *Appl. Catal., A*, 2005, **281**, 225–231.
38 Y. Kusunoki, T. Miyazawa, K. Kunimori and K. Tomishige, *Catal. Commun.*, 2005, **6**, 645–649.
39 T. Miyazawa, Y. Kusunoki, K. Kunimori and K. Tomishige, *J. Catal.*, 2006, **240**, 213–221.
40 T. Miyazawa, S. Koso, K. Kunimori and K. Tomishige, *Appl. Catal., A*, 2007, **318**, 244–251.
41 G. Zhang, W. Guan, H. Shen, X. Zhang, W. Fan, C. Lu and W. Shi, *Ind. Eng. Chem. Res.*, 2014, **53**, 5443–5450.
42 N. Li, H. Teng, L. Zhang, J. Zhou and M. Liu, *RSC Adv.*, 2015, **5**, 95394–95400.